High Performance Polymer Nanowire Field-Effect Transistors with Distinct Molecular Orientations

Chengyi Xiao, Guangyao Zhao, Andong Zhang, Wei Jiang, René A. J. Janssen, Weiwei Li, Wenping Hu,* and Zhaohui Wang**

Semiconducting polymer field-effect transistors (FETs) have been widely investigated because of their broad applicability in future organic circuits, such as radio frequency identification tags, flexible displays, electronic paper, electronic skin, and sensors. These applications use some of the key features of polymer semiconductors, such as flexibility, light weight, easy fabrication, and low cost.[1–4] Using extensively optimized conjugated polymers with tailored energy levels and crystallinity, polymer FETs have successfully achieved high hole (>10 $cm^2 V^{-1} s^{-1}$),[5–8] electron (>5 $cm^2 V^{-1} s^{-1}$),[9] and ambipolar mobilities above 1 $cm^2 V^{-1} s^{-1}$,[10–12] exceeding typical amorphous silicon-based FETs. The charge carrier mobility of polymer FETs strongly depends on the chemical structure of conjugated polymer,[13] the device configuration and interface,[14,15] and polymer microstructures.[16] It is widely reported that conjugated polymers have the strong tendency to self-assemble into nanostructures due to the strong π–π interaction between polymer chains. The stacking provides facile channels for enhancing interchain charge transport and improving the mobility of charges.[17–24] Among these nanostructures, conjugated polymer nanowires exhibit high mobilities up to 24 $cm^2 V^{-1} s^{-1}$,[25] indicating their great potential for application in FETs.

Crystalline polymer nanowires can be prepared by a variety of methods, such as self-seeding method,[26,27] solvent vapor annealing,[20,28–30] direct writing,[31] and templated and templateless assembly.[32–34] The rigid conjugated repeat units provide these polymers with the tendency to self assemble into long crystalline fibers via strong noncovalent interchain or intrachain interactions. Interestingly, most conjugated polymer nanowires used for FETs exhibit an "edge-on" configuration with the π-stacking direction parallel to the substrate,[23,35] whereas the "face-on" configuration with π-stacking direction perpendicular to the substrate is rarely reported.[17,36] It is an issue of debate whether the "edge-on" alignment is beneficial for charge hopping between different chains to the electrode, as some investigations indicate that the charge carriers in FETs are only present in the first molecular layers on the substrate.[37,38] Therefore, the "face-on" configuration that conjugated polymer backbone is more close to the substrate will be helpful for charge movement to the electrode and yield higher carrier mobility.[39] To clarify these concerns, it will be very important to explore the polymer nanowires with "face-on" configurations.

In this work, we use two diketopyrrolopyrrole (DPP) based conjugated polymers with similar molecular structures to fabricate polymer nanowire FETs, in which the polymer chains are present in either an "edge-on" or a "face-on" orientation. DPP polymers have been widely applied in high performance thin film FETs because of their semi-crystalline nature.[40,41] Only, few studies on DPP polymer nanowire FETs have been reported and in these studies, the polymer chains showed exclusively "edge on" orientation.[23,25] In this contribution, we study two conjugated polymers that both consist of decyltetradecyl (DT) substituted DPP and benzodithiophene (BDT) repeat units, but are linked via different aromatic heterocycles, viz., thiophene (T) or thiazole (Tz). This minor structural modification has a major influence on the orientation of the polymer in the nanowires and on the charge carrier mobilities. Remarkably, the polymer orientation is completely switched from "edge on" to "face on" in the nanowires and both polymers give high hole mobilities >5 $cm^2 V^{-1} s^{-1}$, indicating these two stacking configurations are equally good for charge transport. In addition, the thiazole-bridged DPP polymer nanowires exhibit high and well-balanced ambipolar hole and electron mobilities (5.47 and 5.33 $cm^2 V^{-1} s^{-1}$), among the highest reported ambipolar FETs to the best of our knowledge.[9,42,43]

The chemical structures of the DPP polymers are shown in **Figure 1**. The two polymers consist of electron-deficient DT-substituted DPP and electron-rich BDT repeat units alternating along the chain, connected via thiophene or thiazole. PDPP2TBDT[44] and PDPP2TzBDT[45] have previously been used as electron donor in polymer solar cells with fullerenes as electron acceptor, affording power conversion efficiencies (PCEs) of 6.9% and 3.2%. The relatively low PCE for the PDPP2TzBDT based solar cell originates from a low-lying lowest unoccupied molecular orbital (LUMO) that results in a reduced LUMO offset between the polymer and fullerene compared to PDPP2TBDT. This hinders efficient photoinduced electron transfer and charge generation in polymer solar

Dr. C. Xiao, Dr. G. Zhao, Dr. A. Zhang, Dr. W. Jiang, Prof. W. Li, Prof. W. Hu, Prof. Z. Wang
Beijing National Laboratory for Molecular Sciences
Key Laboratory of Organic Solids
Institute of Chemistry
Chinese Academy of Sciences (ICCAS)
Beijing 100190, P. R. China
E-mail: liweiwei@iccas.ac.cn; huwp@iccas.ac.cn; wangzhaohui@iccas.ac.cn
Dr. C. Xiao, Dr. G. Zhao, Dr. A. Zhang
School of Chemistry and Chemical Engineering
University of Chinese Academy of Sciences
Beijing 100049, P. R. China
Prof. R. A. J. Janssen
Molecular Materials and Nanosystems
Eindhoven University of Technology
P.O. Box 513, 5600 MB Eindhoven, The Netherlands

DOI: 10.1002/adma.201502617

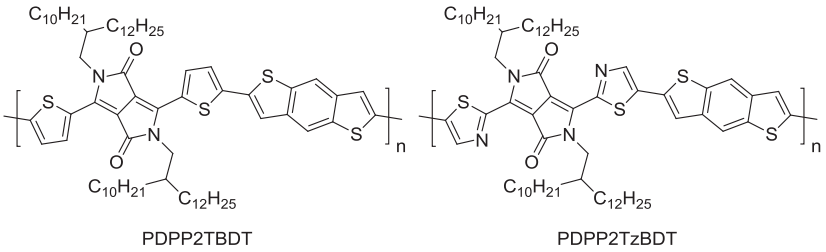

Figure 1. The DPP polymers PDPP2TBDT and PDPP2TzBDT used in this work.

cells. On the other hand, this low-lying LUMO level is beneficial for electron injection from an Au electrode in FETs. The selected DPP polymers have very high molecular weights (M_w > 100 kg mol^{-1}) and form fibrillar structures in bulk-heterojunction systems when blending with fullerene derivatives.

Polymer nanowires of PDPP2TBDT and PDPP2TzBDT were prepared by a facile in-situ drop-coating method in which the polymers are dissolved in the dilute chloroform ($CHCl_3$) solution (0.01 mg mL^{-1}). To ensure homogenous growth of the nanowires ortho-dichlorobenzene (*o*-DCB) was used as a high-boiling point additive (5 vol%) to the volatile chloroform. This $CHCl_3$:*o*-DCB mixture is identical to solvent system used to cast the photoactive layers of polymer-fullerene solar cells, but the initial polymer concentration is about thousand times less. The polymer nanowires can be easily obtained, when drops of the polymer solutions were deposited onto Si/SiO_2 substrates treated with n-octyltrichlorosilane (OTS) and left to dry.

The shape of the polymer nanowires was evaluated using optical microscopy (OM), scanning electron microscopy (SEM), and tapping-mode atomic force microscopy (AFM) (**Figure 2**). Both PDPP2TBDT and PDPP2TzBDT form homogenous and long nanowires (>70 μm) with widths of 0.15–0.4 μm as shown in OM images (Figure 2a,b). SEM images on large scale (50 and 200 μm), presented in the Supporting Information (Figure S1), show that these well-defined nanowires are spatially dispersed over the entire surface area. OM shows that in addition to the well-defined polymer nanowires, irregular shaped particles form during the evaporation process as present in the Supporting Information (Figure S2a,b). It is important to mention that, at higher concentrations of the polymer in the solution (such as 0.1 and 1 mg mL^{-1}) the polymer nanowires can also be formed. However under these conditions, the nanowires are surrounded by a thin polymer film (Figure S2c–f, Supporting Information), which hampers the fabrication of single polymer nanowire FETs. The dimensions of the polymer nanowires were further examined by SEM and AFM, which confirm the measurement from OM images. The narrow and long polymer nanowires formed in dilute solutions (0.01 mg mL^{-1}) provide the possibility to construct FETs by depositing Au electrodes on top and using the substrate as a gate.

High-resolution transmission electron microscopy (TEM) images of representative single polymer nanowires and the corresponding selected area electron diffraction (SAED) patterns enable a more detailed understanding of the fibrillar crystal structure and molecular packing motif in the polymers (**Figure 3**a,b). The PDPP2TBDT nanowires exhibited single-crystal characteristics with diffraction spots equivalent to a repeating distance of 5.46 Å (014) along the polymer main chain direction, which was further confirmed by density functional theory (DFT) calculations as presented in Figure S3a (Supporting Information). The (010) diffraction spot with distance of 3.63 Å indicates the π–π stacking between the polymer chains. The appearance of (010) and (014) spots reveals that the PDPP2TBDT chains are aligned parallel to the longitudinal wire axis and the alkyl side chains are oriented perpendicular to the substrate ("edge on"). The result can be further confirmed by 1D out-of-plane X-ray diffraction measurement (XRD) (Figure 3c), where the (100) diffraction peak was found with the distance of 21.9 Å, corresponding to the lamellar packing distance associated with the alkyl side chains. The molecular orientation of PDPP2TBDT in the polymer nanowire is quite similar to that of PDTTDPP in which DPP is copolymerized with dithieno[3,2-b:2′,3′-d]thiophene linked via thiophene units.[23]

PDPP2TzBDT with thiazole-bridges also presents a similar (005) diffraction spot with 4.13 Å that is related to the length of the repeat units of Tz-DPP-Tz-BDT (Figure S3b, Supporting Information), indicating that the polymer chain is also along the nanowire. Different from PDPP2TBDT, the (600) diffraction spot is found in the SAED pattern (Figure 3b) at 3.17 Å, which due to the lamellar stacking of alkyl side chains with distance of 19.02 Å. It is interesting to note that, out-of-plane XRD measurements on PDPP2TzBDT thin films show the (100) diffraction peak at 23.7 Å (Figure S4, Supporting Information), indicating that a more dense polymer chain packing can be realized in the nanowire than in the film. From the SAED measurement, it can be inferred that the π–π stacking of the polymer conjugated backbone is perpendicular to the substrate ("face-on"). This result is further confirmed by an out-of-plane XRD measurement for the PDPP2TzBDT nanowires (Figure 3d), showing different diffraction peaks compared to that of the PDPP2TBDT nanowires (Figure 3c). The (100) diffraction peak has disappeared, but the (010) and (020) diffraction peaks are present. The (020) diffraction peaks with the distance of 3.47 Å are correlated to the π–π stacking of the polymer backbone.

From TEM, SAED, and XRD measurement, we conclude that PDPP2TBDT and PDPP2TzBDT are present different molecular orientation on the surface. PDPP2TBDT favors the typical edge-on packing motif but PDPP2TzBDT has a face-on configuration (Figure 3e). The molecular packing in polymer nanocrystals could be deduced as an orthorhombic crystal unit cell with lattice constants: $a \approx 21.9$ Å, $b \approx 3.63$ Å, $c \approx 21.84$ Å for PDPP2TBDT and $a \approx 19.02$ Å, $b \approx 6.94$ Å, $c \approx 20.65$ Å for PDPP2TzBDT. PDPP2TzBDT seems to show smaller lattice constants, indicating that replacing of thiophene bridges by thiazole bridges results in forming a condensed crystal structures, that will be useful for charge transport in organic FETs.

FETs were fabricated to study the charge transport in the polymer nanowires. Bottom-gate top-contacted FETs were constructed on an OTS (octadecyltrichlorosilane) modified Si/SiO_2 substrate (n-type Si wafer containing 300 nm-thick SiO_2) using an "organic ribbon mask" technique,[46] which was performed on a Micromanipulator 6150 probe station with a

Adv. Mater. **2015**,
DOI: 10.1002/adma.201502617

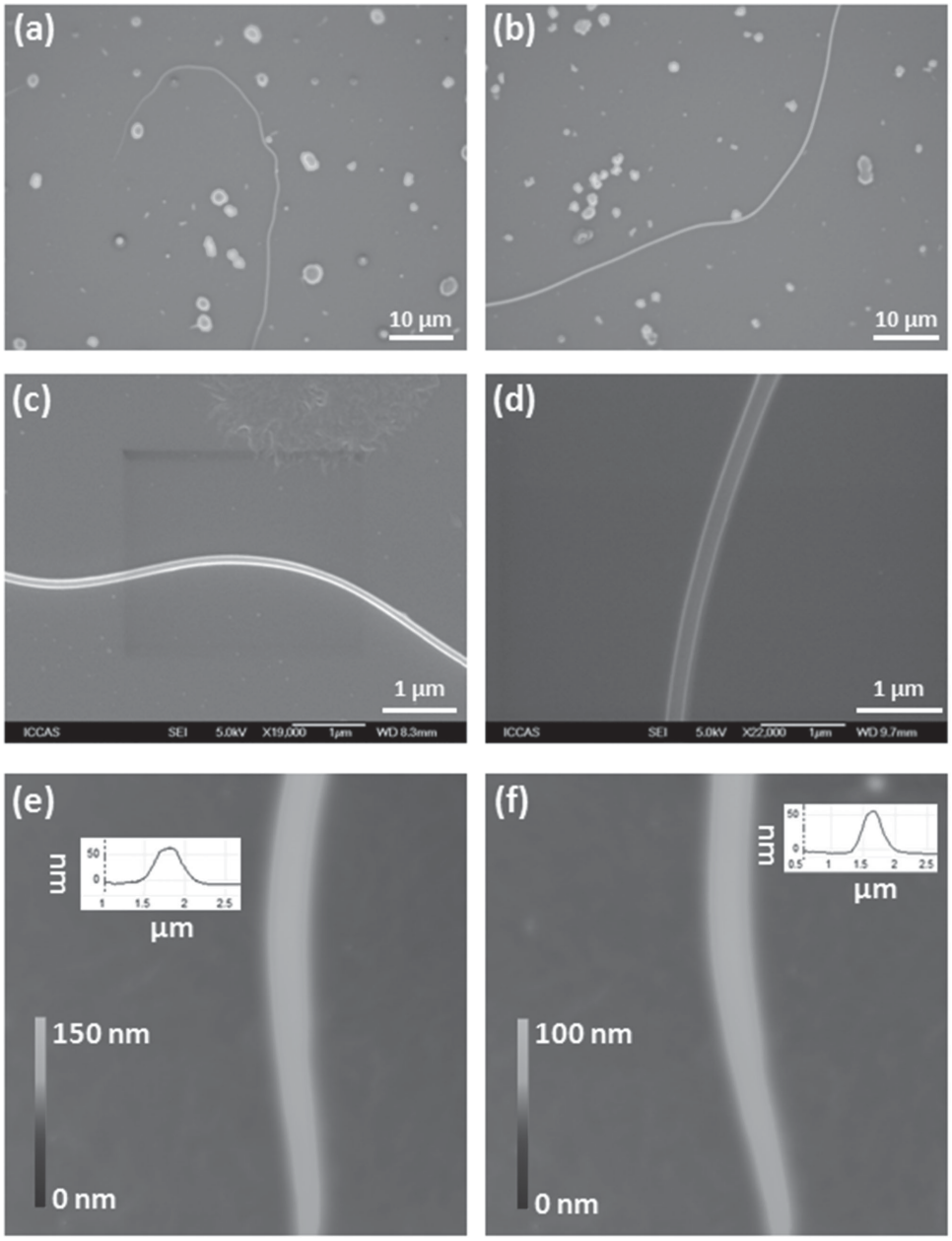

Figure 2. a,b) OM, c,d) SEM, and e,f) AFM images of the polymer nanowires self-assembled on OTS treated Si/SiO_2 substrates in dilute $CHCl_3$ with 5% *o*-DCB solution. Panels (a,c,e) are for PDPP2TBDT, and (b,d,f) are for PDPP2TzBDT.

high resolution microscopy (magnification at 400–1000 times) (Figure S5, Supporting Information). As a comparison, top-contact bottom-gate thin film FET devices (width = 200 μm, length = 25 μm) were fabricated in a higher concentration (4 mg mL^{-1}) through spin-coating. The polymer nanowire FETs based on the two polymers showed similar channel width (0.53–0.64 μm) and length (5.21–6.33 μm), which is much smaller than the thin films FET devices. PDPP2TBDT nanowires present high hole mobility of 7.42 $cm^2\ V^{-1}\ s^{-1}$ but a relatively low electron mobility of 0.04 $cm^2\ V^{-1}\ s^{-1}$ (**Figure 4** and **Table 1**), which may be attributed to the high-lying LUMO levels (–3.81 eV) of the polymers that hinders electron injection. For PDPP2TzBDT, with a much deeper LUMO levels of –4.0 eV as a result of replacing thiophene by thiazole in the main chain, the polymer nanowires FETs show ambipolar charge transport with well-balanced hole and electron mobilities of 5.47 and 5.33 $cm^2\ V^{-1}\ s^{-1}$. The result is among the highest for balanced ambipolar organic FETs based on conjugated polymers reported so far. It is important to note that, thin films FETs show comparatively low charge mobilities, with $\mu_h = 0.72\ cm^2\ V^{-1}\ s^{-1}$ and $\mu_e = 0.0034\ cm^2\ V^{-1}\ s^{-1}$ for PDPP2TBDT and $\mu_h = 0.14\ cm^2\ V^{-1}\ s^{-1}$ and $\mu_e = 0.11\ cm^2\ V^{-1}\ s^{-1}$ for PDPP2TzBDT (Table 1 and Figure S6, Supporting Information). These results demonstrate that the polymer crystalline nanowires with well-ordered

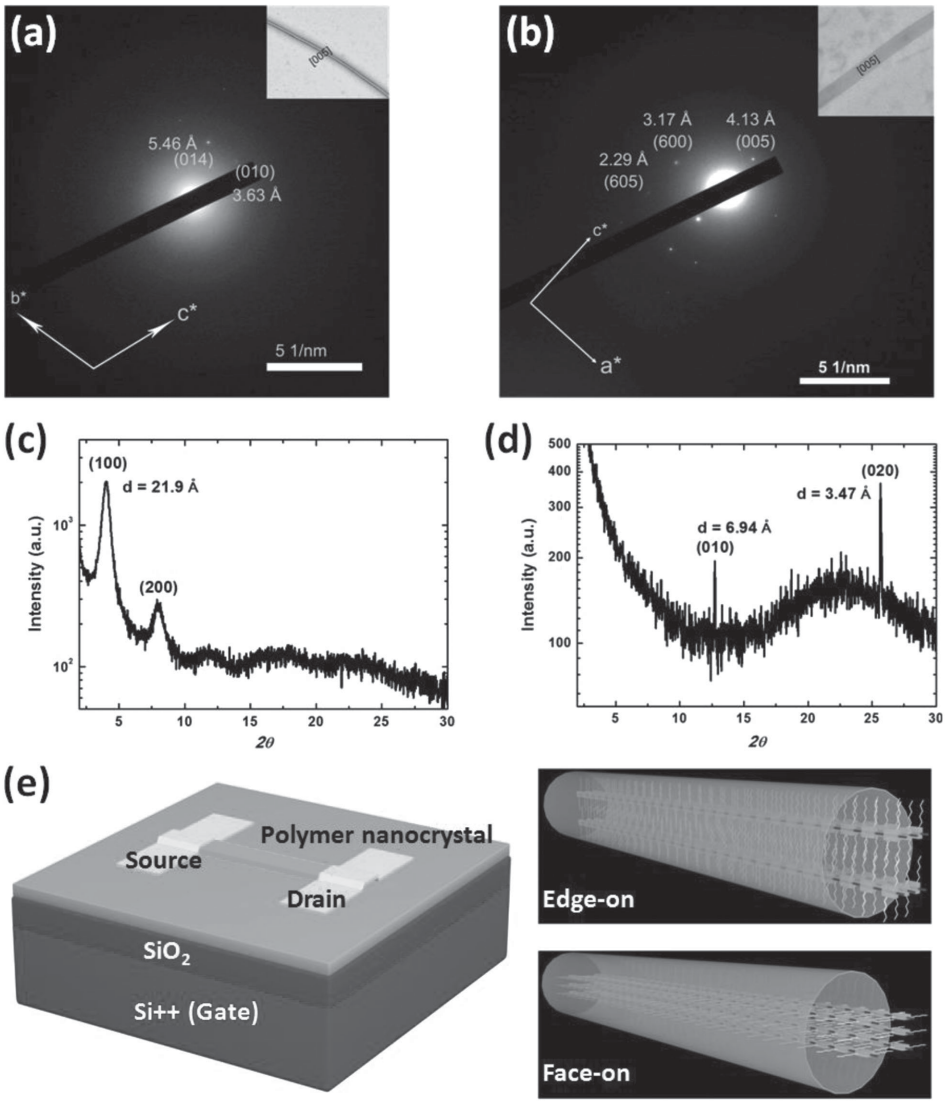

Figure 3. a,b) TEM images of the polymer nanowires and their corresponding SAED patterns. c,d) 1D out-of-plane XRD profiles of the polymer nanowires. a,c) For PDPP2TBDT and b,d) for PDPP2TzBDT. e) Schematic diagram of PDPP2Tz-BDT nanowire transistors and molecular packing in the 1D nanocrystals.

molecular conformation are beneficial for charge transport and therefore provide much better carrier mobility, which is mainly attributed to the reduced structural and energetic disorder.[47] It has also been reported that charge transport along the polymer backbone is one to two orders of magnitude faster than that along the π–π direction.[48,49] Therefore, the polymer chains that are aligned along the nanowire direction would be partially responsible for the high carrier mobility of the polymer nanowire FETs compared to thin film FETs. It is also important to point out that these results show that both "edge-on" and "face-on" molecular orientations can provide high mobility in the polymer nanowire FETs, which is also observed in thin films transistors.[39,50]

In conclusion, two conjugated polymers with similar chemical structures were used to grow polymer nanowires for organic FETs. When the linker units between the DPP core and the benzodithiophene units are altered from thiophene to thiazole, the DPP polymers show distinctly different molecular orientation on the surface from "edge-on" to "face-on" configuration, and both polymer nanowire FETs present high charge mobilities up to 7.42 $cm^2\ V^{-1}\ s^{-1}$. The different molecular orientation, but with similar chemical structures, will further be useful to study the intrinsic charge transport properties in organic FETs.

Experimental Section

The conjugated polymers were synthesized according to the literature procedures.[44,45]

The substrates used here were successively cleaned with pure water, piranha solution (H_2SO_4/H_2O_2 = 7:3), pure water, pure isopropyl alcohol, and finally blown dry with high-purity nitrogen gas. Treatment of the

Adv. Mater. 2015,
DOI: 10.1002/adma.201502617

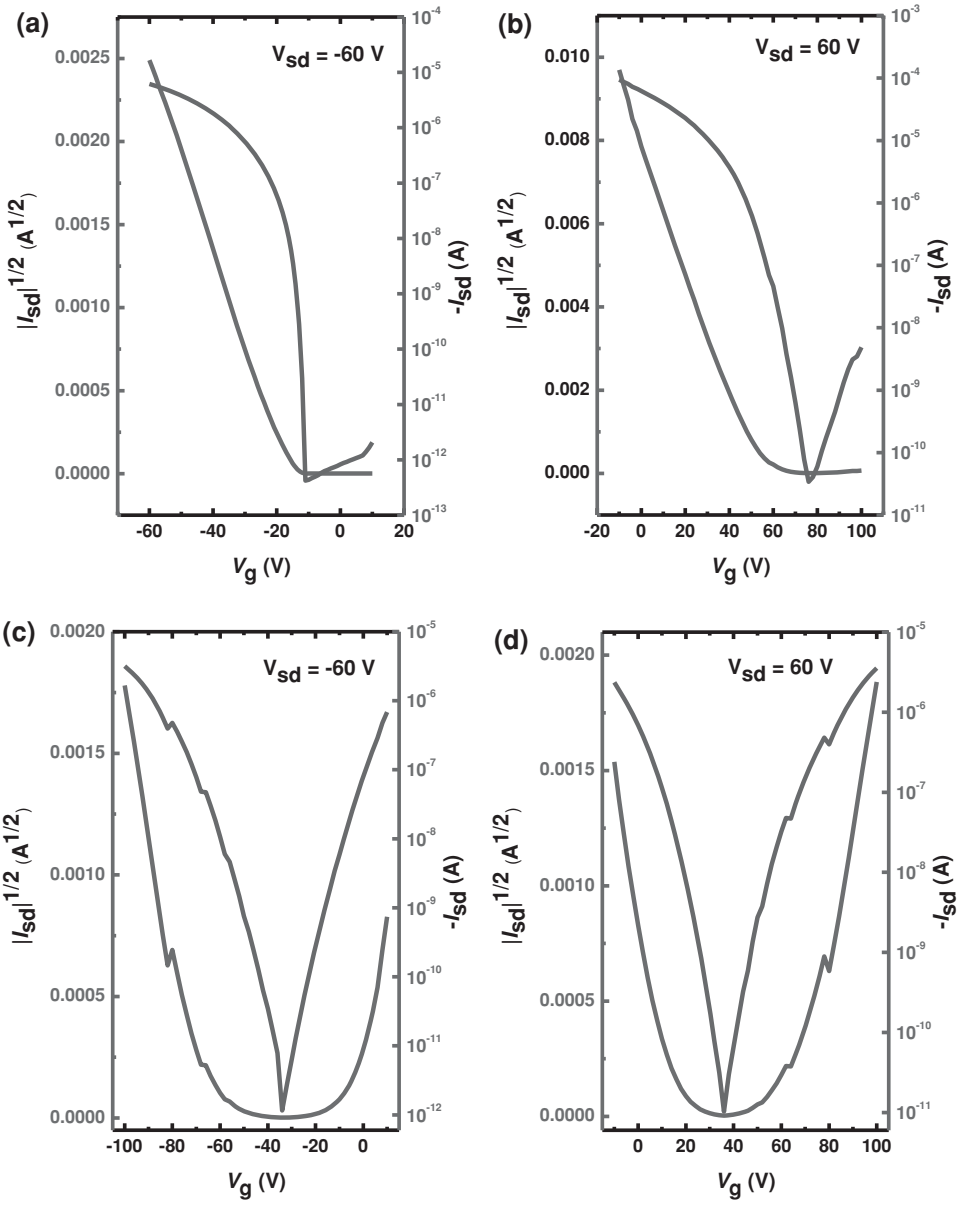

Figure 4. a,c) p-Type and b,d) n-type transfer characteristics for the DPP-polymer-nanowire-based FETs with top contact configuration: a,b) for PDPP2TBDT, c,d) for PDPP2TzBDT.

Table 1. Field-effect hole (h) and electron (e) mobility of the DPP polymer thin films and nanowires (NW).

Polymer		Mobility [$cm^2 V^{-1} s^{-1}$]	V_T [V]	On/off ratio
PDPP2TBDT	Thin Film (h)	0.72	−22.3	10^5
	Thin Film (e)	0.0034	71.2	10^2
	NW (h)	7.42	−19.7	10^6
	NW (e)	0.04	69.8	10^2
PDPP2TzBDT	Thin Film (h)	0.14	−67	10^6
	Thin Film (e)	0.11	65	10^6
	NW (h)	5.47	−60.4	10^5
	NW (e)	5.33	60.1	10^5

Si/SiO_2 wafers with OTS was carried out by the vapor-deposition method. The clean wafers were dried under vacuum at 90 °C for 0.5 h in order to eliminate the influence of moisture. When the temperature decreased to 70 °C, a small drop of OTS was placed around the wafers. Subsequently, this system was heated to 120 °C and maintained for 2 h under vacuum.

Polymer nanowires were fabricated by the use of an additive (5 vol% *o*-DCB) in a dilute $CHCl_3$ solution (0.01 mg mL^{-1}). Bottom-gate top-contact OFETs based on the polymer nanowires were constructed on an OTS modified Si/SiO_2 substrate (n-type Si wafer containing 300 nm-thick SiO_2) using an "organic ribbon mask" technique. Prior to the self-assembly of polymer nanowires, the OTS modified Si/SiO_2 substrate was cleaned with pure n-hexane, pure chloroform, and pure isopropyl alcohol. Then, polymer nanowires were produced on Si/SiO_2 substrates through drop casting. Subsequently, 40 nm thick source and drain electrodes were deposited on the nanowires by thermal evaporation with an organic ribbon as the mask. For the thin film OFETs, polymer thin films were spin coated on the substrate from chloroform solution with thickness

around 30–50 nm and then moved into high vacuum chamber for thermal annealing at corresponding temperature for 2 h (160 °C for PDPP2TBDT and 175 °C for PDPP2TzBDT). Electrical characteristics of the devices were recorded with a Keithley 4200-SCS semiconductor parameter analyzer and a Micromanipulator 6150 probe station in a glove box at room temperature. The mobilities were calculated from the saturation region with the following equation: $I_{DS} = (W/2L)C_i\mu(V_G - V_T)^2$, where I_{SD} is the drain–source current, W is the channel width, L is the channel length, μ is the field-effect mobility, C_i is the capacitance per unit area of the gate dielectric layer, and V_G and V_T are the gate voltage and threshold voltage, respectively. This equation defines the important characteristics of electron mobility (μ), on/off ratio ($I_{on/off}$), and threshold voltage (V_T), which could be deduced by the equation from the plot of current–voltage.

The microscope images of all the aligned microcrystal arrays were acquired by an optical microscope (Vision Engineering Co., UK), which was coupled to a CCD camera. AFM measurements were carried out with a Nanoscope IIIa instrument (Digital Instruments). XRD was measured on a D/max2500 with a CuK_α source (λ = 1.541 Å). SEM images were obtained with a Hitachi S-4300 microscope (Japan), and TEM observation was carried out with a JEOL 1011 microscope.

Supporting Information

Supporting Information is available from the Wiley Online Library or from the author.

Acknowledgements

This work was supported by the Recruitment Program of Global Youth Experts of China. The work was further supported by the National Natural Science Foundation of China (21225209, 91427303, 21474026), the 973 Program (2011CB932301, 2014CB643600, 2013CB933500), and the Strategic Priority Research Program (XDB12010100) of the Chinese Academy of Sciences. The research forms part of the Solliance OPV programme and has received funding from the Ministry of Education, Culture and Science (Gravity program 024.001.035) of the Netherlands.

Received: June 2, 2015
Revised: June 29, 2015
Published online:

[1] a) C. Wang, H. Dong, W. Hu, Y. Liu, D. Zhu, *Chem. Rev.* **2012**, *112*, 2208; b) X. Zhao, X. Zhan, *Chem. Soc. Rev.* **2011**, *40*, 3728.
[2] H. N. Tsao, K. Mullen, *Chem. Soc. Rev.* **2010**, *39*, 2372.
[3] A. J. Heeger, *Chem. Soc. Rev.* **2010**, *39*, 2354.
[4] H. Sirringhaus, *Adv. Mater.* **2014**, *26*, 1319.
[5] I. Kang, H.-J. Yun, D. S. Chung, S.-K. Kwon, Y.-H. Kim, *J. Am. Chem. Soc.* **2013**, *135*, 14896.
[6] J. Y. Back, H. Yu, I. Song, I. Kang, H. Ahn, T. J. Shin, S.-K. Kwon, J. H. Oh, Y.-H. Kim, *Chem. Mater.* **2015**, *27*, 1732.
[7] C. Luo, A. K. K. Kyaw, L. A. Perez, S. Patel, M. Wang, B. Grimm, G. C. Bazan, E. J. Kramer, A. J. Heeger, *Nano Lett.* **2014**, *14*, 2764.
[8] G. Kim, S.-J. Kang, G. K. Dutta, Y.-K. Han, T. J. Shin, Y.-Y. Noh, C. Yang, *J. Am. Chem. Soc.* **2014**, *136*, 9477.
[9] B. Sun, W. Hong, Z. Yan, H. Aziz, Y. Li, *Adv. Mater.* **2014**, *26*, 2636.
[10] Y. Zhao, Y. Guo, Y. Liu, *Adv. Mater.* **2013**, *25*, 5372.
[11] H. Chen, Y. Guo, Z. Mao, G. Yu, J. Huang, Y. Zhao, Y. Liu, *Chem. Mater.* **2013**, *25*, 3589.
[12] Z. Y. Chen, M. J. Lee, R. S. Ashraf, Y. Gu, S. Albert-Seifried, M. M. Nielsen, B. Schroeder, T. D. Anthopoulos, M. Heeney, I. McCulloch, H. Sirringhaus, *Adv. Mater.* **2012**, *24*, 647.
[13] Y. Olivier, D. Niedzialek, V. Lemaur, W. Pisula, K. Müllen, U. Koldemir, J. R. Reynolds, R. Lazzaroni, J. Cornil, D. Beljonne, *Adv. Mater.* **2014**, *26*, 2119.
[14] R. P. Ortiz, A. Facchetti, T. J. Marks, *Chem. Rev.* **2010**, *110*, 205.
[15] C. Liu, Y. Xu, Y.-Y. Noh, *Mater Today* **2015**, *18*, 79.
[16] M. Mas-Torrent, C. Rovira, *Chem. Rev.* **2011**, *111*, 4833.
[17] H. Sirringhaus, P. J. Brown, R. H. Friend, M. M. Nielsen, K. Bechgaard, B. M. W. Langeveld-Voss, A. J. H. Spiering, R. A. J. Janssen, E. W. Meijer, P. Herwig, D. M. de Leeuw, *Nature* **1999**, *401*, 685.
[18] J. A. Merlo, C. D. Frisbie, *J. Phys. Chem. B* **2004**, *108*, 19169.
[19] A. L. Briseno, S. C. B. Mannsfeld, P. J. Shamberger, F. S. Ohuchi, Z. Bao, S. A. Jenekhe, Y. Xia, *Chem. Mater.* **2008**, *20*, 4712.
[20] H. Dong, S. Jiang, L. Jiang, Y. Liu, H. Li, W. Hu, E. Wang, S. Yan, Z. Wei, W. Xu, X. Gong, *J. Am. Chem. Soc.* **2009**, *131*, 17315.
[21] X. Xiao, Z. Wang, Z. Hu, T. He, *J. Phys. Chem. B* **2010**, *114*, 7452.
[22] Y. Wu, B. Su, L. Jiang, A. J. Heeger, *Adv. Mater.* **2013**, *25*, 6526.
[23] J. H. Kim, D. H. Lee, D. S. Yang, D. U. Heo, K. H. Kim, J. Shin, H.-J. Kim, K.-Y. Baek, K. Lee, H. Baik, M. J. Cho, D. H. Choi, *Adv. Mater.* **2013**, *25*, 4102.
[24] Y. Liu, H. Dong, S. Jiang, G. Zhao, Q. Shi, J. Tan, L. Jiang, W. Hu, X. Zhan, *Chem. Mater.* **2013**, *25*, 2649.
[25] H. A. Um, D. H. Lee, D. U. Heo, D. S. Yang, J. Shin, H. Baik, M. J. Cho, D. H. Choi, *ACS Nano* **2015**, *9*, 5264.
[26] J. Y. Oh, M. Shin, T. I. Lee, W. S. Jang, Y. Min, J.-M. Myoung, H. K. Baik, U. Jeong, *Macromolecules* **2012**, *45*, 7504.
[27] J. Xu, Y. Ma, W. Hu, M. Rehahn, G. Reiter, *Nat. Mater.* **2009**, *8*, 348.
[28] X. Xiao, Z. Wang, Z. Hu, T. He, *J. Phys. Chem. B* **2010**, *114*, 7452.
[29] Y. Liu, H. Dong, S. Jiang, G. Zhao, Q. Shi, J. Tan, L. Jiang, W. Hu, X. Zhan, *Chem. Mater.* **2013**, *25*, 2649.
[30] Y. Liu, H. Wang, H. Dong, L. Jiang, W. Hu, X. Zhan, *Small* **2013**, *9*, 294.
[31] B. W. Maynor, S. F. Filocamo, M. W. Grinstaff, J. Liu, *J. Am. Chem. Soc.* **2002**, *124*, 522.
[32] G. A. O'Brien, A. J. Quinn, D. A. Tanner, G. Redmond, *Adv. Mater.* **2006**, *18*, 2379.
[33] J. Liu, Y. Lin, L. Liang, J. A. Voigt, D. L. Huber, Z. R. Tian, E. Coker, B. McKenzie, M. J. McDermott, *Chem. Eur. J.* **2003**, *9*, 604.
[34] D. H. Kim, Y. D. Park, Y. Jang, S. Kim, K. Cho, *Macromol. Rapid Commun.* **2005**, *26*, 834.
[35] S. H. Wang, M. Kappl, I. Liebewirth, M. Muller, K. Kirchhoff, W. Pisula, K. Müllen, *Adv. Mater.* **2012**, *24*, 417.
[36] L. Li, Y. Yu, G. J. Ye, Q. Ge, X. Ou, H. Wu, D. Feng, X. H. Chen, Y. Zhang, *Nat. Nanotechnol.* **2014**, *9*, 372.
[37] S. Fabiano, C. Musumeci, Z. Chen, A. Scandurra, H. Wang, Y. L. Loo, A. Facchetti, B. Pignataro, *Adv. Mater.* **2012**, *24*, 951.
[38] L. Li, Y. Yu, G. J. Ye, Q. Ge, X. Ou, H. Wu, D. Feng, X. H. Chen, Y. Zhang, *Nat. Nanotechnol.* **2014**, *9*, 372.
[39] J. Rivnay, M. F. Toney, Y. Zheng, I. V. Kauvar, Z. H. Chen, V. Wagner, A. Facchetti, A. Salleo, *Adv. Mater.* **2010**, *22*, 4359.
[40] C. B. Nielsen, M. Turbiez, I. McCulloch, *Adv. Mater.* **2013**, *25*, 1859.
[41] Z. Yi, S. Wang, Y. Liu, *Adv. Mater.* **2015**, *27*, 3589.
[42] J. Lee, A. R. Han, H. Yu, T. J. Shin, C. Yang, J. H. Oh, *J. Am. Chem. Soc.* **2013**, *135*, 9540.
[43] B. Sun, W. Hong, H. Aziz, Y. N. Li, *Polym. Chem.* **2015**, *6*, 938.
[44] W. Li, K. H. Hendriks, A. Furlan, W. S. C. Roelofs, M. M. Wienk, R. A. J. Janssen, *J. Am. Chem. Soc.* **2013**, *135*, 18942.
[45] W. Li, K. H. Hendriks, A. Furlan, M. M. Wienk, R. A. J. Janssen, *J. Am. Chem. Soc.* **2015**, *137*, 2231.
[46] L. Jiang, J. Gao, E. Wang, H. Li, Z. Wang, W. Hu, L. Jiang, *Adv. Mater.* **2008**, *20*, 2735.
[47] R. Noriega, J. Rivnay, K. Vandewal, F. P. V. Koch, N. Stingelin, P. Smith, M. F. Toney, A. Salleo, *Nat. Mater.* **2013**, *12*, 1038.
[48] R. A. Street, J. E. Northrup, A. Salleo, *Phys. Rev. B* **2005**, *71*, 165202.
[49] Y. K. Lan, C. I. Huang, *J. Phys. Chem. B* **2009**, *113*, 14555.
[50] X. Zhang, L. J. Richter, D. M. DeLongchamp, R. J. Kline, M. R. Hammond, I. McCulloch, M. Heeney, R. S. Ashraf, J. N. Smith, T. D. Anthopoulos, B. Schroeder, Y. H. Geerts, D. A. Fischer, M. F. Toney, *J. Am. Chem. Soc.* **2011**, *133*, 15073.